Nuclear Engineering and Technology 54 (2022) 644–652

Contents lists available at ScienceDirect

Nuclear Engineering and Technology

journal homepage: www.elsevier.com/locate/net

Original article

Investigation of neural network-based cathode potential monitoring to support nuclear safeguards of electrorefining in pyroprocessing

Young-Eun Jung [a], Seong-Kyu Ahn [b], Man-Sung Yim [a, *]

[a] Department of Nuclear and Quantum Engineering, Korea Advanced Institute of Science and Technology, 291 Daehak-ro, Yuseong-gu, Daejeon, 34141, Republic of Korea

[b] Advanced Fuel Cycle System Research Division, Korea Atomic Energy Research Institute, 111 Daedeok-daero 989beon-gil, Yuseong-gu, 34057, Daejeon, Republic of Korea

ARTICLE INFO

Article history:
Received 6 May 2021
Received in revised form
7 July 2021
Accepted 16 August 2021
Available online 25 August 2021

Keywords:
Pyroprocessing
Process monitoring
Safeguards
Electrorefining
Cathode potential
Electro-deposition
Machine learning

ABSTRACT

During the pyroprocessing operation, various signals can be collected by process monitoring (PM). These signals are utilized to diagnose process states. In this study, feasibility of using PM for nuclear safeguards of electrorefining operation was examined based on the use of machine learning for detecting off-normal operations. The off-normal operation, in this study, is defined as co-deposition of key elements through reduction on cathode. The monitored process signal selected for PM was cathode potential. The necessary data were produced through electrodeposition experiments in a laboratory molten salt system. Model-based cathodic surface area data were also generated and used to support model development. Computer models for classification were developed using a series of recurrent neural network architectures. The concept of transfer learning was also employed by combining pre-training and fine-tuning to minimize data requirement for training. The resulting models were found to classify the normal and the off-normal operation states with a 95% accuracy. With the availability of more process data, the approach is expected to have higher reliability.

1. Introduction

Pyroprocessing is an electrochemical recycling technology for used fuels. As an alternative to aqueous technologies, it has several advantages. Most importantly, it prevents pure plutonium separation, thus provides inherent proliferation resistance in nuclear materials handling. At the same time, due to the difficulty in applying conventional nuclear materials accountancy, pyroprocessing demands advanced methods of nuclear safeguards [1,2].

Conventional nuclear safeguards methods mainly rely on a mass balance-based nuclear material accountancy using sample extraction and destructive assay (DA). However, an inherent uncertainty in materials balance remains when these methods are applied to pyroprocessing. First, a sample obtained from the input stream is not representative because the input is not entirely homogenized. Second, due to continuous accumulation of processed materials, it is impractical to cleanup the mass balance areas where nuclear material accounting is implemented. This causes difficulty in meeting the IAEA's requirement on timely detection of the loss of a significant quantity of special nuclear materials. Responding to this need, new approaches and technologies to enhance existing safeguards are being developed.

For any planned pyroprocessing facility, in order to observe the state of facility operation, significant amounts of operation-related data will be collected. The use of the collected data in process diagnosis is referred to as process monitoring (PM). One possible avenue to contribute to enhancing nuclear safeguards of pyroprocessing is to use PM to supplement existing safeguards approaches [3–6]. With the use of near real time data of the process from PM, it is possible to indirectly track the flow of special nuclear materials (SNMs), constituting more robust safeguards approach. Another advantage of using PM for safeguards purposes is that the facility will require very little to no system reconfiguration for data acquisition. With the use of appropriate data collecting equipment, sufficient amount of operation-related data can be collected to support PM. Accordingly, PM is expected to help increasing confidence in the safeguards for SNMs, lengthening the allowable inventory period, requiring a much smaller number of samples for inspection, and reducing false positive indications [7].

* Corresponding author.
E-mail address: msyim@kaist.ac.kr (M.-S. Yim).

https://doi.org/10.1016/j.net.2021.08.020

The objective of this research is to examine the feasibility of enhancing pyroprocessing safeguards by utilizing PM along with machine learning technique. To support the objective, a cathode potential produced during electrorefining (ER) is selected as a target process signal. Artificial neural network (ANN) method was applied as a tool to process the PM data. The research backgrounds are explained in detail in the following section. Accordingly, an ER operation state between normal and off-normal is determined in the study using an ANN based classifier by observing a cathode potential. To achieve the goal, two separate studies were conducted: 1) Data acquisition by electrodeposition experiments to obtain cathode potential data in normal and off-normal ER conditions, and 2) Development of ANN based classifiers. The following sections describe these two studies.

2. Research background

2.1. Electrorefining and its safeguards

The electrorefining (ER) process is the main unit process in pyroprocessing. In the ER process, a variety of SNMs, such as plutonium, are dissolved into a molten salt electrolyte from used fuels and accumulated in the electrolyte. Depending on the purpose, different designs of ER can be used. For example, one or more solid cathodes can be employed to separate uranium in ER, or uranium can be separated on a solid cathode while the actinides are separated on a liquid cathode.

During ER, only uranium is electro-deposited on a solid cathode due to the differences in equilibrium potentials among the existing elements. Uranium ions oxidize active elements, mainly lanthanide and actinide elements during ER process. These active elements gradually accumulate in the molten salt. In the early stages of operation, about 10 wt% of UCl_3 is added to the system as a starting material [8] and needs to be periodically replenished to prevent a decrease in the uranium concentration. Therefore, it is necessary to monitor whether adequate quantities of elements, including uranium and plutonium, are maintained, to ensure consistent ER operation.

Various ER sensors are available to measure physical properties (temperature, pressure, electrolyte level, rotation speed) and electrical properties (current, voltage, potential). Electrochemical or spectroscopic methods can also be used to determine concentrations of SNM in the electrolyte. Use of additional sensors where nuclear material diversion could occur or is suspected can also be considered based on the consideration of possible off-normal scenarios [9].

Occurrences of undeclared or unexpected situations can result in off-normal operation, countering to the aim of the ER process. Examples of off-normal operational state of ER include leakage of materials, such as salt or gases (chlorine), loss of the inert atmosphere required for successful ER operation, or electrodeposition of unexpected metal on a cathode. While the first two phenomena are related to safety or process robustness rather than safeguards, the last one has direct relevance to nuclear safeguards. In normal ER operating conditions, co-deposition of uranium and plutonium rarely occurs given the difference in their reduction potentials. However, theoretically, co-deposition of the elements on a cathode can occur when the plutonium concentration in the molten salt is high enough as the relative difference in reduction potential between the two elements is not very large. In addition, when the supplied current is inappropriately high, the increased current density of the cathode can drive co-deposition.

2.2. Cathode potential for electrorefining safeguards

To determine the presence of the adequate quantities of these elements in the ER operation, several PM approaches have been suggested. These approaches include potentiometric sensors [10], multi-bubblers [11,12], cyclic voltammetry (CV) [13,14], Laser-Induced Breakdown Spectroscopy (LIBS) [15–18], neutron counter [19], combining a neutron counter and CV [20], and multivariate analytical techniques for voltammetric data [21]. While these approaches can be utilized to detect plutonium co-deposition on a cathode or to determine the change in actinide (plutonium) composition in the molten salt, difficulty commonly arises in measuring the concentration of plutonium separately from the electrolyte mixture containing various species of other actinides and fission products.

Another signal available for the PM approach is cathode potential. In fact, measured data on cathode potential provide a simpler approach to plutonium codeposition detection. Cathode potential is an electric signal recorded while metal ions are reduced to metal on a cathode. The cathode potential is defined as follows by the Nernst equation:

$$\mathrm{E} = E^{0\prime} + \frac{RT}{nF}\ln(C_{\mathrm{ox}}) \quad (1)$$

where E is the electrode potential [V], $E^{0'}$ is the standard apparent reduction potential [V], R is the ideal gas constant [8.314 J/mol·K], T is the absolute temperature [K], n is the number of electrons involved in the oxidation-reduction reaction, F is the Faraday's constant [96,485 C/mol], and C_{ox} is the concentration of the reacting oxidants [mol/cm^3].

The electrode potential is influenced by the variations in both temperature (T) and the concentration of oxidants (C_{ox}). Theoretically, since standard reduction potential is a thermodynamic property of each element and differs from element to element, it is possible to infer whether the process operation is in a normal state (pure uranium deposition) or off-normal state (co-deposition) by examining the changes in cathode potential. During pure uranium deposition, the potential is maintained at a constant value. However, if other active elements start to deposit, the potential will shift to a more negative value.

Examining cathode potential for nuclear safeguards purposes has been considered in combination with modeling approaches. Rappleye et al. [22] developed a computer code called, DREP (Deposition Rates from Electrode Potential), to predict U, Pu, and Zr deposition on the cathode and the element deposition rates by analyzing cathode potential and cell current. Three types of operating modes were simulated in the code: U deposition, U/Pu codeposition, and U/Zr codeposition. Since Pu has a more negative reduction potential than U, when the cathode potential is more negative than pure U deposition, DREP predicts less U deposition and more Pu deposition. Also, if cathode potential is less negative than pure U deposition, Zr codeposition is predicted. The instantaneous deposition rates calculated during a batch could be used to estimate the final composition of the cathode deposits. Although validation of the code is not complete, DREP has provided the theoretical basis for real-time PM of the solid cathode product in ER by utilizing measurable process readings, cathode potential and cell current, to predict the deposition behavior at the cathode.

Shannon and Simpson [23] also suggested cathode potential as a promising PM indicator based on a study of abnormal operation detection in electrorefining using ERAD [24]. They simulated diversion scenarios in which the ER process continued without

refilling UCl_3, and showed an increase in U–Pu codeposition as the cathode potential decreased. While this simulation-based research used extremely high current (more than 140 A) and a number of uncontrolled cycles (about 30) to reach a codeposition-possible condition (U–Pu ratio), the method indicates applicability of cathode potential to safeguards of ER.

Sakamura et al. conducted electrowinning (EW) experiments to study codeposition of uranium and plutonium onto an inert solid cathode in LiCl–KCl eutectic salt containing UCl_3 and $PuCl_3$ [25]. EW is a process used to recover actinides and lanthanides after ER. Though the purposes of EW and ER are different, the processes are based on the same principles of electrochemistry. By using both potentiostatic and galvanostatic electrolysis, the research showed actual responses of cathode potential based on the deposited elements and examined the behavior of U–Pu codeposition with respect to concentration ratio and cathodic current density. When the EW process was conducted at a cathodic current density higher than the limiting current density of U^{3+} reduction, Pu was initially codeposited with U. However, the electrode surface area increased with the deposition of U–Pu metal, which facilitated U deposition. This phenomenon was observed in chronopotentiograms of LiCl–KCl–UCl_3-$PuCl_3$ eutectic salt.

According to the literature, use of cathode potential for nuclear safeguards of ER appears promising. However, the actual electrode potential is the result of the complex and diverse interactions of various elements in molten salt. As these interactions are affected by the exchange current densities of elements (which depend on their concentrations), current density (which is affected by the mass transfer of elements), and the continuous change of concentration and cathode surface area, actual measurements of the cathode potential signal can easily get complicated [26]. Therefore, to determine the deposited elements on a cathode, a statistical approach is often implemented to analyze the monitored data of the cathode potential.

2.3. Machine learning in nuclear safeguards

Another key issue addressed in this research is to use machine learning for safeguards applications. Machine learning is widely recognized as a tool to effectively manage and utilize massive amounts of data. In machine learning, existing data are used to enable a computer to learn how to conduct a given task by means of statistical inference, without explicit programming.

AI or machine learning has been applied in nuclear safeguards since the 1990's. In 1994, Menlove et al. developed the software Video Time and Radiation Analysis Program (VTRAP) to automatically review and analyze continuous safeguards data from unattended monitoring systems using pattern recognition by neural networks [27]. Two types of data, C/S video and NDA sensor, were used for monitoring the movement of nuclear material to distinguish normal material movements from off-normal activity. Experiments were conducted to collect data to train the neural network for pattern recognition. The results showed that VTRAP can successfully distinguish between normal and off-normal data, which indicates the feasibility of applying AI to nuclear safeguards.

Along with wide adaptation of computing techniques, a number of research projects applied machine learning techniques to nuclear industry for improving safety, security, and safeguards. Machine learning is also being applied to PM research in order to improve the robustness of the process operations. Some have also proposed the application of machine learning to enhance pyroprocessing safeguards. Recently, Shoman et al. suggested the use of machine learning for pyroprocessing safeguards to classify off-normal operations by employing PM (mass measurements) and NDA (nondestructive assay, e.g., gamma spectroscopy measurements) [28]. They simulated the data from running a computer code - the Separations and Safeguards Performance Model (SSPM) [29] and tested the feasibility of such approach by using a support vector machine (SVM). They emphasized the importance of unsupervised learning in safeguards, since it eliminates the burden of identifying all possible diversion pathways with acquisition of the corresponding data. The SVM detected not only normal operation but also both direct and substitution diversion.

An artificial neural network (ANN) is a well-known machine learning technique. Thanks to the development of rapidly enhanced computing techniques, ANN has been widely developed and many ANN based architectures exist. Since ANN mimics human brain function, simple components of ANN are neurons and connections between the neurons. By varying the connections between neurons to neurons and neurons to layers, a variety of NN architectures have been developed. Representative architectures are a convolution neural network (CNN) and recurrent neural network (RNN). Depending on their specific purpose, those architectures are commonly used in a variety of fields.

Pouri et al. examined the analysis of CV data to predict unseen data sets (previously unencountered situations) by implementing an ANN technique [30]. By using the data sets' interrelation between variables, ANN was trained in the study to mimic the ER's electrochemical cell system thus to provide simulated CV data sets. To develop an ANN structure and validate the prediction results, published experimental data [31] were applied which was obtained using 0.5–5 wt% of zirconium chloride ($ZrCl_4$) in LiCl–KCl molten salt with different scan rates at 773 K. In each experimental data set, the input data consisted of potential, process time, concentrations and scan rates; the current was produced as output. About 43% of the total experimental data were used as training data. ANN's predictive ability and limitations were examined by using the remaining data set having different conditions (concentrations and scan rates). This study indicated that ANN has good predictive capability and a strong potential for application in safeguards for pyroprocessing.

3. Experimental design for data collection

A series of electrodeposition experiments were designed and conducted with various cell compositions to produce cathode potential data in lab-scale. The experiments involved both single-element deposition (normal operation) and two-element codeposition (off-normal operation). Three lanthanides (Lns), La, Ce, and Gd, with small differences in standard reduction potentials were used as surrogate materials. This produces a favorable environment for codeposition according to the order of reduction potential, $E_{Gd} > E_{Ce} > E_{La}$. Accordingly, Gd or Ce (higher reduction potential) is deposited first, followed by La. In the experiments, two types of binary systems were employed; one using lanthanum - cerium (La–Ce) and the other using lanthanum - gadolinium (La–Gd). Both systems produced normal (single deposition) and off-normal (co-deposition) data. Data were labeled based on the composition of the deposits after being analyzed using inductively coupled plasma atomic emission spectroscopy (ICP-OES). The composition of electrochemical cells was designed the same way as in previous research [20]; for more details and general descriptions of the experiments, see reference 20. Only a brief explanation of each experimental cell design is provided here.

Codeposition of two elements occurs when equilibrium potentials of the elements are close. According to the Nernst equation (Eqn. (1)), the difference in equilibrium potentials can be adjusted by using the mole ratio of the electrolyte components. Differences in electrode potential were varied from 0.00 to 0.15 V. The range of

equilibrium potential differences was designed to be between 0.00 and 0.10 V for the Ce–La binary system and between 0.05 and 0.15 V for the Gd–La binary system. A total of six experimental cells was used. Considering that the electrolyte in an actual electrorefiner is initially about 10 wt% UCl_3, the experimental cells were also designed to contain approximately 10 wt% $GdCl_3$-$LaCl_3$ or $CeCl_3$–$LaCl_3$. An electrodeposition experiment was also conducted in a cell containing 10 wt% $LaCl_3$ to obtain a pure singular deposition signal. The designed electrochemical cells are presented in Table 1.

The experiments for producing cathode potential during electrodeposition (both singular deposition and co-deposition) were conducted in a glove box in an inert atmosphere with less than 1 ppm of both oxygen and moisture. To allow room for dendrite growth, a large furnace (SKUTT, KM-614, US) was employed and located inside the glove box. The operating temperature was maintained at 773 K (±3 K) as measured with a chromel-alumel thermocouple.

The electrochemical cell used in the experiments consisted of three electrodes in a molten salt bath: a working electrode, a counter electrode, and a reference electrode. The working electrode was a molybdenum wire with a 1 mm diameter (99.94%, Alfa Aesar). This electrode was immersed 2 (±0.2) cm into the molten salt. The counter electrode was an Ln metal (Ln = La, Ce, or Gd, 99.9%, Alfa Aesar) rod located in a stainless steel basket. These two electrodes were sheathed in alumina tubes to prevent electrical conduction between materials. A Ag/AgCl reference electrode was prepared using 1 wt% AgCl (99.997%, Alfa Aesar) in a LiCl–KCl eutectic salt with a silver wire (0.5 mm diameter, 99.9985%, Alfa Aesar), contained in a thin mullite tube (4 mm inner diameter, 6 mm outer diameter). To prepare an electrolyte consisting of 59-41 mol% LiCl–KCl eutectic salt, LiCl (>99%, ACS, Alfa Aesar) and KCl (>99%, ACS, Alfa Aesar) were mixed in an alumina crucible and heated at 773 K for more than 3 h to remove any moisture. After the cell cooled down, $LnCl_3$ (99.9%, ultry dry, Alfa Aesar) was added to the mixture, which was then reheated to adjust the final molten salt concentrations (See Table 1). A schematic of the electrochemical cell is shown in Fig. 1.

A constant electric current was applied and the cathode potential was recorded for 600 s. To vary the deposition ratio, the supplied current was varied from 100 to 500 mA in 50 mA intervals. Each experiment was repeated at least 3 times. The bottom of the cathode that was sheathed in alumina was surrounded by a basket allowing capture of any fallen deposits. This minimized the loss of electrodeposited material as shown in Fig. 1. A potentiostat/galvanostat (Biologic, SP-150) was used in conjunction with EC-lab software in the electrodeposit experiments.

After each experiment, the electrodeposits and the eutectic salts were sampled and analyzed for their quantities and associated compositions using ICP-OES (Agilent, Agilent ICP-OES 5110). The electrodeposit samples were prepared by cutting the bottom of the Mo electrode which contained the deposited lanthanides. The

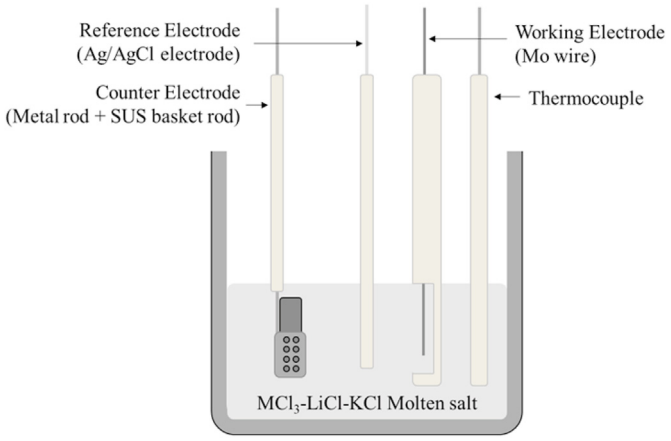

Fig. 1. Electrochemical cell design for experiments.

samples were weighed and then dissolved in 20 ml of 10% HNO_3. Since 10% HNO_3 cannot dissolve Mo metal, the Mo was collected from the acid solution and weighed in order to subtract its weight from the initial sample weight. Further dilution was conducted to ensure the sample concentration was between 0.1 and 10 ppm. The final acidity of ICP-OES samples was maintained at 2% HNO_3. The salt sample was weighed and then dissolved in 20 ml of 2% HNO_3. The salt analysis results were used to remove the effect of deposited salt in determining the codeposition ratio. Ln contained in the salt was subtracted from the quantity of deposits quantity.

4. Results of electrodeposition experiment and data labeling for cathode potential

4.1. Feature of cathode potential data

Fig. 2 shows the cathode potential data from a Ce 1 cell when the supplied current is 500 mA. This experimental condition was one of the most codeposition favorable environments. As shown in Fig. 2, the cathode potential, after the initial drop, gradually increases as electrodeposition takes place. Such gradual increase is due to a reduction in the current density on the cathode as the cathodic surface area enlarges with the growth of deposits. The initial rapid reduction in cathode potential occurs because all of the reactants surrounding the electrode are consumed by the instantaneous electrodeposition as the supply of electric current begins. The electrode potential increases as the concentration gradient stabilizes over time through diffusion and as the cathodic surface area grows. The cathode potentials steadily reach a plateau after a rapid initial increase, which was confirmed through additional experiments conducted for 120 min.

As mentioned before, electrode potential is the outcome of various complex interactions in electrochemistry involving

Table 1
The compositions of each electrochemical cells in the electrodeposition experiments.

ΔE [V]	$CeCl_3$–$LaCl_3$ Binary System				$GdCl_3$-$LaCl_3$ Binary System			
	Cell Name	$CeCl_3$ [mol] (wt%)	$LaCl_3$ [mol] (wt%)	X_{Ce}/X_{La}	Cell Name	$GdCl_3$ [mol] (wt%)	$LaCl_3$ [mol] (wt%)	X_{Gd}/X_{La}
–	La0	–	0.160 (10.0%)	–				
0.00	Ce1	0.015 (0.90%)	0.145 (9.00%)	0.1	–			
0.05	Ce2	0.080 (4.90%)	0.080 (4.90%)	1	Gd1	0.032 (2.1%)	0.128 (7.9%)	0.25
0.10	Ce3	0.145 (9.00%)	0.015 (0.90%)	10	Gd2	0.114 (7.5%)	0.046 (2.8%)	2.5
0.15	–				Gd3	0.154 (10.1%)	0.006 (0.4%)	25

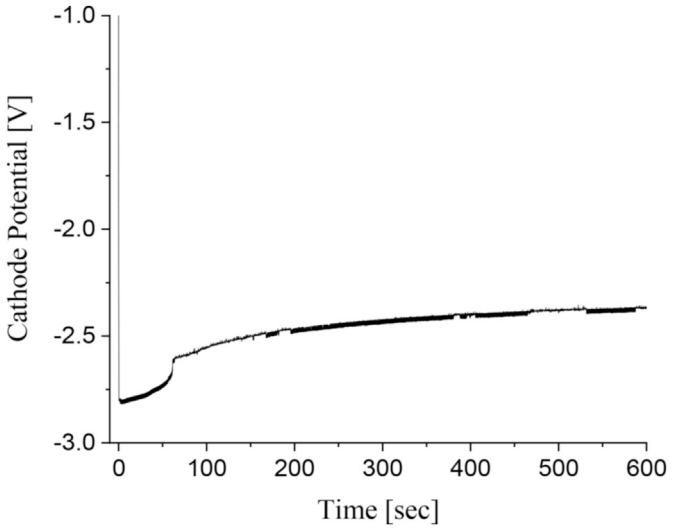

Fig. 2. A graph of a cathode potential obtained in Ce 1 cell (0.9 wt% $CeCl_3$ and 9.0 wt% $LaCl_3$) by applying 500 mA.

electrolyte and electrode. As these interactions are strongly affected by the current density of the cathode, current density is a key factor to the electrodeposition reaction. Furthermore, from a microscopic viewpoint, the thickness of the diffusion layer is also a factor that affects the deposition. The diffusion layer affects the amount of current and the rate of oxidation-reduction of the reactants and causes non-uniform deposition on the cathode due to the heterogeneity of the molten salt. Other factors such as time-dependent changes in cathode surface area and concentrations of the species in the electrolyte also affect the deposition, resulting in the cathode geometry becoming complex. These interactions proceed continuously over time with variations in the local conditions. Even though experiments are conducted repeatedly under the same experimental conditions, cathode potentials do not result in the same pattern but only similar patterns due to the randomness of the process.

An electrode reaction consists of an electron transfer to the electrode surface and a mass transfer through diffusion, transporting the reactants from the electrolyte to the surface of the electrode. The electron transfer is faster as the over-voltage increases, whereas the speed of the diffusion-controlled reactant transfer is independent of the over-voltage, driven by the concentration gradient between the electrode surface and the solution. Therefore, when the over-voltage is large enough, the current is determined by diffusion and cannot be increased beyond a certain value. This value is called “limiting current.” If the supplied current is greater than the limiting current, there is a lack of reactants (element A) near an electrode which cannot be recovered by diffusion. Therefore, another element (element B) having a more negative reduction potential than element A is deposited along with element A [25], leading into codeposition.

4.2. Data labeling

The codeposition ratios measured for each of the experimental cells are presented in Table 2. As mentioned, when the electrode potential difference is small, two elements are deposited together. In the Ce 1 cell, where the electrode potential difference was zero, La which has a more negative electrode potential than Ce was deposited in greater quantities than Ce. The Ln electrodeposits often got detached from the electrode, because the Ln deposition had a weak attachment to the Mo electrode. When an electrodeposit fell to the bottom of the alumina tube, recovery and analysis of the sample was very difficult. This detachment phenomenon was more serious in the Gd–La binary cells than in the Ce–La binary cells. Due to the difficulty in obtaining precise data, a range of the codeposition ratios based on sample DA analysis was assigned to each experimental cell.

The varied co-deposition ratios resulted from the complexity of the electrochemical reaction (reduction) is reflected in the observed cathode potentials. The measured codeposition ratios were used label the data as normal (singular deposition) or off-normal (co-deposition) to support the employment of machine learning. Since it is possible to have a small amount of codeposition due to high electrode current density at an early stage, the sample was classified as normal when the codeposition ratio was very small (less than 5%). The result of data labeling is shown in Table 3. In total, the number of normal and off-normal data were 82 and 118, respectively.

5. Computational model development

In this section, the data preprocessing method and the approach to ANN based model development are explained. In model development, cathode potential data were preprocessed for use as input data to address the quantity and quality issues in the raw data. In the training of the computational model, transfer learning technique was used as a method of pre-training and fine-tuning. Firstly, a model was pre-trained using singular La data and the binary La–Ce data. Then, the pre-trained model was re-trained (fine-tuned) using only normal La–Gd data. The retrained model was tested to distinguish operation states from both normal and off-normal La–Gd data.

Table 3
Data labeling (grouping) method and the resulted number of data.

Data type	Data acquisition environment	Data labeling	The number of cathode potential data
Normal	La singular cell	N_La	27
	Ce–La binary cell	N_Ce	27
	Gd–La binary cell	N_Gd	28
Off-normal	Ce–La binary cell	O_Ce	29 + 30 = 59
	Gd–La binary cell	O_Gd	27 + 32 = 59

Table 2
The results of electrodeposition experiment: Co-deposition ratio and the number of cathode potential data according to each electrochemical cell.

Cell	Codeposition ratio: La/Ce	The number of cathode potential data (the number of DA result)	Cell	Codeposition ratio: La/Gd	The number of cathode potential data (the number of DA result)
La 0	–	27 (27)			
Ce 3	<5%	27 (5)	Gd 3	<1%	28 (16)
Ce 2	40–60%	29 (8)	Gd 2	10–25%	27 (14)
Ce 1	300–1200%	30 (18)	Gd 1	100–300%	32 (24)

5.1. DATA preprocessing

A key to using machine learning is to prepare appropriate data in both quantity and quality. In the case of quantity, due to the nature of machine learning, a large number of data are desired. Through electrodeposition experiments, two hundred data of cathode potential were collected, with each data point covering 10-min interval. To increase sample size, the data covering each 10-min interval were further divided into ten 1-min subinterval data. Since the collected data are time-sequential and data slicing was conducted sequentially, integrity and the features of the experimental data were not compromised with data slicing. Fig. 3 shows the cathode potential data (same as in Fig. 2) on a logarithmic scale. The cathode potential decreased within the first 60 s and then increased which signifies codeposition of two different elements. This phenomenon has been observed in constant-current coulometry where each variation corresponds to a specific reduction potential [32]. The data from the first 1-min interval were discarded to eliminate the effect of initial reactants reduction on the cathode which is not related to the electrotransport related deposition in the system.

The next step in data preprocessing was necessary to address the data quality issue. As cathode potential represents the outcome of various electrochemical reactions in the system, the measured cathode potential value itself does not reveal some of the details needed for the intended electrodeposition analysis. As a key parameter in controlling the kinetics of the electrochemical reactions, changes in current density affect the electrodeposition rate. For example, the cathode potential gradually increases during the electrodeposition process as shown in the results. These increases are due to the decrease in current density caused by increased cathodic surface area.

Describing the effect of current density changes is considered in the study by adding cathodic surface area to the input data. This is by noting the interrelation between cathodic surface area and current density. Under the given experimental setup, however, performing direct measurement of cathodic surface area growth was very difficult. In this study, indirectly representing cathodic surface area growth by using a mathematical relationship given by the Cottrell equation is utilized.

As shown below, the Cottrell equation describes the changes in electric current as a function of time in a controlled potential experiment. The equation is valid when the applied potential is constant and was derived by solving the linear diffusion equation where diffusion governs the mass transfer [33].

$$i = \frac{nFAC_0\sqrt{D}}{\sqrt{\pi t}} \rightarrow A(t) = \frac{i\sqrt{\pi t}}{nFC_0\sqrt{D}} \quad (2)$$

The values of the variables, D (diffusion coefficient) and n (the number of transferred electrons) were obtained from an experimental study on the properties of the electrochemical cell under the same conditions [26]. The equation assumes the electrode surface area remains a constant, which can be valid for a very short-term period. In this study, constant current was supplied for 10 min during the electrodeposition experiments. We also noted that during the 10 min interval, the corresponding potentials remained at almost a constant level. Accordingly, the use of the Cottrell equation to describe the changes in the surface area with electrodeposition is expected to be acceptable within the given time intervals. Then, the tendency for the time-dependent growth of cathodic surface area is given by $A(t) = A_0 + at^{0.5}$ with the difference in the growth rate of the cathodic surface area proportional to the supplied current.

5.2. NEURAL network based classifier development

This study aims to examine whether it is possible to develop a classifier to distinguish between normal and off-normal ER operation using the observations of cathode potential. At the same time, given the sensitive nature of defining the specifics of what is off-normal [28], devising and conducting experiments to obtain comprehensive off-normal ER operation data is a challenge. We attempted to develop such classifier by mainly focusing on using normal data along with the use of limited off-normal data. To support such implementation, we applied the transfer learning approach to machine leaning algorithm development. Transfer learning is a method that uses previous knowledge to solve a new task [34]. If a computer model is capable of performing a given task, it is expected that the model will also be able to conduct a similar but different task as well. In transfer learning, most of the structure of a pre-trained model (layers) is frozen and only a small portion of the existing layers are retrained using a separate set of data.

Transfer learning is a machine *learning* (ML) method that focuses on storing knowledge gained from solving one problem and applying it to a related but different problem. Through transfer learning, a model developed for a task is reused as a starting point with an expectation that it will successfully conduct a similar second task. The advantage of transfer learning is that it can achieve higher accuracy using a small amount of data without requiring the model development process starting from scratch. Thus, a number of runs for trial-and-error optimization can be reduced by adjusting the number of layers and nodes, regularization, and the learning rate.

Transfer learning was utilized in pre-training and fine-tuning of models. By pre-training a model and transferring its knowledge to develop a new model, it is possible to extract features that are common between the models. All of the data obtained from the La singular cell and the Ce–La binary cell (54 normal data and 59 off-normal data from N_La, N_Ce, and O_Ce) were used in model development in pre-training (model A). Since 10 min data were processed as 1 min data with 20 s interval, about 24 data were produced from one cathode potential data. 70% of the data (1900 data) were used for training model A and the rest (800 data) were used for model testing. Model A was saved with its structure frozen and then retrained (or fine-tuned) by adding normal data from Gd–La binary system (28 data of N_Gd). The performance of the

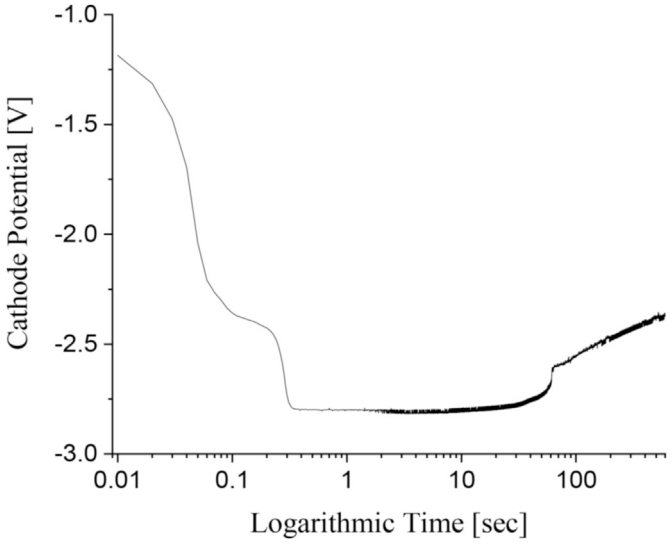

Fig. 3. A logarithmic scale graph of the cathode potential obtained in Ce 1 cell (0.9 wt% $CeCl_3$ and 9.0 wt% $LaCl_3$) by applying 500 mA (the same with Fig. 2).

fine-tuned model (model B) was tested by using off-normal data from Gd–La binary system (59 data in O_Gd).

The reason why La–Ce data were used for pre-training was because of smaller difference in standard reduction potential between La and Ce ($\Delta E = 0.05$ V) in comparison to the difference between La and Gd ($\Delta E = 0.08$ V). By being able to classify a signal that has small reduction potential differences between the elements, it would be easier to distinguish the signals produced by elements having larger standard reduction potential differences (i.e., U and Pu with $\Delta E = 0.3$ V).

In developing a classifier model through pre-training and fine-tuning, this study employed a convolutional neural network (CNN) to support the feature representation learning. A CNN serves the purpose of filtering and captures specific features in the data by repeating a convolution layer and a pooling layer. Therefore, CNN allows extraction of important features with reduction in the input dimensions.

Based on the features extracted from CNN, a classification model was developed using a recurrent neural network (RNN). A RNN captures the sequential information present in the input data and provides an algorithm to process the time sequential data (time-series data) collected in the study. To find the most suitable structure, this study also examined several types of RNN including (a standard) RNN, long short-term memory (LSTM), and bidirectional LSTM (Bi-LSTM). In case of (a standard) RNN, each node (neuron) saves previous data in memory so as to relate them with newly introduced data, and combine the data sequentially. However, as the time steps increase, data cannot be transferred effectively. LSTM is a type of RNN that facilitates sequential data transfer by adding a cell state as special units in addition to standard units of RNN. Each node in LSTM is a memory cell consisting of an input gate, an output gate, and a forget gate. Through these gates, the amount of data used in learning is controlled. Accordingly, LSTM is expected to show better performance than (a standard) RNN for handling long sequential input. Bi-LSTM learns the time-sequential data in two directions (past and future), therefore, is useful for learning long term bi-directional dependency in sequential data. However, in general, as computational steps become more complicated, Bi-LSTM requires higher computing costs.

With the selected architectures, the models for classification were developed by adjusting suitable hyper-parameters, including the number of layers and nodes, learning rate, and batch size. The models were optimized with respect to classification accuracy and computation time by using optimization algorithms such as Adam, SDG, and AMSGrad.

To determine the impact of the length of time data, the data slicing interval (observation time) was varied between 2 and 3 min. These variations, however, did not produce a discernible difference in the results. Two different ways of using the cathode surface area were also tested in model development with the data produced by using the Cottrell equation: 1) to cover the entire time periods of the electrodeposition; 2) to cover only the early electrodeposition periods; and 3) not using the data at all. Using the cathodic surface area only for the initial period of electrodeposition is based on recognizing the difficulty in describing complex dendrite growth behaviors in later period. This approach also assumes that use of the cathodic surface area data during the initial fast growth period may facilitate the learning of the model for the ensuing time sequential data.

Based on model optimization, the RNN based model was developed consisting of 4 layers of RNN having 256 nodes in each layer. In the case of the LSTM and Bi-LSTM based models, both have 3 layers of LSTM or Bi-LSTM, with each layer consisting of 128 nodes. All three models used 2 layers of CNN for extracting features from the input data. The softmax function was employed in the final layer of a neural network-based classifier. The overall concept of model development procedure and structure of the developed models is shown in Fig. 4.

6. Classification results and discussions

As explained, development of the classification models was based on different uses of the cathodic surface area data. First, when the cathodic surface area data are not used as input, none of the models achieved more than 70% accuracy in pre-training. This may indicate the importance of using the cathode surface area data in developing a pre-trained model leading to an accurate fine-tuned model. This also indicates that using only the cathode potential data does not provide enough information necessary to capture the trends in time-dependent changes of electrodeposition. This also implies the necessity of taking into account the changes in cathodic current density in describing the cathode potential.

When the cathodic surface area data was used in the pre-training stage covering the entire time periods of the electrodeposition, the models achieved the accuracy level at lower than 80%. After sequential fine-tuning, the models performed poorly (less than or about 50% accuracy level). In contrast, when the cathodic surface area data was used only for the initial electrodeposition period, the models achieved more than 95% accuracy in pre-training. After the fine-turning, the models with initial cathodic surface area data also successfully classified off-normal data from the test data set: The models using RNN and LSTM were more than 90% accurate and the Bi-LSTM based model achieved about 83% accuracy. The standard deviation of test results (conducted five times as part of fine-tuning of the models) were 3.9, 6.8, and 6.1 for RNN, LSTM, and Bi-LSTM, respectively.

To improve the performance of the classifier models, “ensemble averaging” was also applied to the developed models. The ensemble average technique uses multiple evaluations in classification and combines the results in final determination (off-normal data vs. normal data). The results are summarized in Table 4.

The higher accuracy achieved with the use of the initial cathode surface area data derived from the Cottrell equation indicates that using such data directly contributes to classifying normal and off-normal data in the study. However, the data derived from the Cottrell equation for the entire periods of cathode area changes were not found useful in the classification. This raises the question of why second approach does not improve the classification accuracy. The answer may be due to the fact that the growth of cathode surface area is stochastic and becomes increasingly complex with time. Such random growth feature is due to various factors such as, local differences in current distributions, reactant (electrolyte) fluid flows, nonuniform dendrite formations, and fracture developments. Moreover, dendrite shape differs from element to element with variations in element properties [25,35]. Given these variations, the derived surface area value from the Cottrell equation

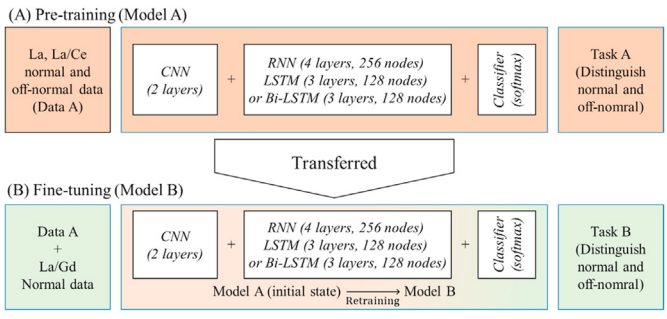

Fig. 4. Model development procedure and structure of the developed models.

Table 4
Classification accuracy (%) of the developed models in distinguishing off-normal data.

		Following sequential surface area			Focusing initial rapid change		
		RNN	LSTM	Bi-LSTM	RNN	LSTM	Bi-LSTM
Pre-training		65–70	75–80	75–80	>95%	>95%	>95%
Fine tuning	1	35.6	34.1	55.0	95.8	96.7	86.9
	2	38.5	31.2	76.2	90.4	96.2	85.1
	3	40.3	38.1	49.2	90.0	89.5	71.3
	4	32.1	31.0	52.8	85.5	97.6	82.9
	5	37.9	38.5	48.6	96.0	79.5	88.6
Average		36.9	34.6	56.3	91.5	91.9	82.9
Standard deviation		2.83	3.25	10.19	3.94	6.82	6.14
Ensemble					96.4	95.8	87.1

at a given time is inherently limited in representing the actual situation.

At an initial stage, electrodeposition occurs rather uniformly since the electrode surfaces are smooth with the influence of local variations at a minimum. In this case, the dendrite growth characteristics may be controlled by the dominant features of the given electrochemical system. Then, the cathodic surface area and the corresponding current density represented by the Cottrell equation were relevant to describe the electrodeposition behavior. However, the similar data from the Cottrell equation in the later time periods was incapable of explaining the electrodeposition behavior in the cathode due to mounting complexities in random local condition variations.

In this study, lanthanide elements were used as surrogates to represent uranium and plutonium in electrorefining. As the lanthanide elements have smaller differences in standard reduction potentials, use of them facilitates the acquisition of codeposition data in the experiment. In actual electrorefining environment, however, codeposition of uranium and plutonium rarely occurs because of their considerable differences in standard reduction potentials. Nevertheless, developing the classification model by using the surrogate elements serves the purpose of this study as the surrogate data well represent the presence of normal or off-normal data.

In terms of defining what is normal (singular deposition) and off-normal (codeposition), the data in pre-training were classified based on the value of the co-deposition ratio: When the codeposition ratio (La/Ce or La/Gd) is less than 5%, the data were labeled as normal data. Use of 5% as the criterion was partly to control the amount of data in two groups in pre-training with balance. In fine-tuning, the normal data was classified with less than 1% codeposition ratio and the model was retrained by using only the normal data. This resulted in a classifier model with performance acceptable against all data including both normal and off-normal data. Even though the data used in this study has limitations in representing the comprehensive scenarios of off-normal operations of electrorefining, the result of this study indicate that the methodology presented is acceptable for the intended applications in nuclear safeguards, i.e., to compensate for the shortcomings of current approaches.

With the ability to learn and retain time-sequential features of the input data, use of the RNN series of architectures was found appropriate to perform pre-training and fine-tuning of the classifier model in the study. The ability of the RNN series of architectures in pre-training the model and solving the second similar task (fine-tuning stage) enabled classifier development using rather small amount of data. It is expected that the model will be further improved with availability of larger amount of data to represent the electrorefining system.

This study showed the use of electrode potential data along with RNN-based machine learning approach can support nuclear safeguards applications for electrorefining operations. However, since the data used in the study are electric signals, they are potentially vulnerable to manipulations. For instance, an operator can induce a false potential by connecting an adjustable resistor. However, in an actual facility, not only cathode potential but other process signals, such as operating temperature and weight of electrode, would be available to detect the occurrence of such unexpected operations. In the case of temperature, the effect of operating temperature on cathode potential is shown in the Nernst equation (eqn. (1)). This indicates that the reliability of PM will increase as long as the relevant data are available, making it very difficult to create spoofing signals [28]. Also, with the increase in the size of the data sets in monitored variables, more reliable machine learning techniques or architecture, such as deep learning, would be applicable. Availability of such data can support the design of facilities under the so-called “safeguards by design (SBD)” approach. Through proper design and planning, the SBD approach could provide reliable nuclear safeguards without requiring additional expense or installation of new equipment. Furthermore, the approach can be applied not only to electrorefining but also to other unit processes in the overall pyroprocessing facility.

Process monitoring is a supplemental technology supporting mass balance-based safeguards approach. The traditional safeguards approach requires an inspector to visit the facility regularly. By applying a reliable PM approach, it is possible to increase confidence in the safeguards without requiring human presence. As a result, it helps to reduce the frequency of inspections (saving safeguards cost) and reduces false positive indications. Consequently, it could lengthen the allowable inventory period in nuclear safeguards, resulting in a reduced number of days of operation shutdown.

7. Conclusions

Given the limitations in current approaches to pyroprocessing safeguards, use of supplemental technology such as process monitoring is needed. In this study, the feasibility of machine learning based process monitoring was examined to develop a novel safeguards approach for pyroprocessing. Cathode potential obtained during electrorefining was selected as the target PM signal. Depending on the electrodeposition status, the operation states of electrorefining were defined as normal (for singular deposition) and off-normal (for codeposition).

To support classification model development, cathode potential data were measured through electrodeposition experiments in three types of molten salt systems: La singular, La–Ce binary, and La–Gd binary cells. The experimental cell compositions were varied to provide favorable conditions for both singular deposition and codeposition. The resulting electrodeposits were analyzed using ICP-OES, and the data were labeled as normal and off-normal, according to the codeposition ratio.

In order to transform the data into proper inputs for machine learning, preprocessing of the data were made. Preprocessing included increasing the number of data points by time slicing, discarding inappropriate data, and adding model based data (cathode surface area) to reduce the effects of unknown features. The concept of transfer learning was applied to pre-training and fine-tuning of models. This approach allows a classifier to require only normal data in development by pre-training. While the acquisition of off-normal data is difficult to support nuclear safeguards applications, transfer learning helps classifier model development in the presence of data limitations.

In the current study, a pre-trained model was developed by using data from La singular and La–Ce binary cells on the basis of standard reduction potentials of each element. The model was then fine-tuned with only normal data from La–Gd binary cells. And the classification accuracy was tested using off-normal data from La–Gd binary cells.

In the model development, a convolution neural network (CNN) was applied to extract features from the input data. A series of recurrent neural network (RNN) architectures were also tried in order to find the most appropriate model. Various trial-and-error based methods were also employed to optimize the model. When RNN and long-short term memory (LSTM) architectures were used, the models provided classification accuracy levels at higher than 95%.

In summary, this research indicates the feasibility of using cathode potential measurement with machine learning to enhance safeguards-ability of pyroprocessing during electrorefining. The approach could also be expanded to other processes in pyroprocessing through process monitoring of relevant variables.

Declaration of competing interest

The authors declare that they have no known competing financial interests or personal relationships that could have appeared to influence the work reported in this paper.

Acknowledgments

This research was supported by National Nuclear R&D Program (Human Resources Program in Energy Technology) through the National Research Foundation of Korea (NRF) by the Ministry of Science, Science and Technology (NRF-2018M2C7A1A02071198).

References

[1] R. Bean, Project Report on Development of a Safeguards Approach for Pyroprocessing, Idaho Natl. Lab., 2010, pp. 1–75. INL/EXT-10-20057.
[2] P.C. Durst, M.H. Ehinger, B. Boyer, I. Therios, R. Bean, A. Dougan, K. Tolk, Advanced Safeguards Approaches for New TRU Fuel Fabrication Facilities, Pacific Northwest Natl. Lab., 2007, pp. 1–65. PNNL-17151.
[3] H.E. Garcia, W.C. Lin, T.S. Yoo, Process Monitoring for Safeguards via Event Generation, Integration, and Interpretation, Idaho Natl. Lab., 2010, pp. 1–10. INL/CON-10-19138.
[4] T. Burr, M. Hamada, C. Orton, Data-driven versus period-driven change detection for process monitoring, in: The 53rd Annual INMM Meeting, Orlando, Florida, July 15-19, 2012.
[5] H.E. Garcia, M.F. Simpson, W.C. Lin, T.S. Yoo, R.B. Carlson, Detecting proliferation activities via system-centric integration and interpretation of multimodal data collected from a system of sensors, in: The 54th Annual INMM Meeting, Atlanta, Georgia, USA, July 20-24, 2013.
[6] B. Cipiti, O. Zinaman, The Integration of Process Monitoring for Safeguards, Sandia Natl Lab., 2010, pp. 1–26. SAND2010-6593.
[7] R. Metcalf, A. Bevill, W. Charlton, R. Bean, Safeguards Envelope: Previous Work and Examples, Idaho Natl. Lab., 2008, pp. 1–9. INL/CON-08-14405.
[8] R.O. Hoover, R.S. Michael, M. Sean, S. Kumar, S. Phongikaroon, Electrochemical studies and analysis of 1–10 wt% UCl_3 concentrations in molten LiCl–KCl eutectic, J. Nucl. Mater. 452 (2014) 389–396.
[9] H.E. Garcia, M.F. Simpson, W.C. Lin, R.B. Carlson, T.S. Yoo, Application of process monitoring to anomaly detection in nuclear material processing systems via system-centric event interpretation of data from multiple sensors of varying reliability, Ann. Nucl. Energy 103 (2017) 60–73.
[10] P.A. Zink, J.F. Jue, B.E. Serrano, G.L. Fredrickson, B.F. Cowan, S.D. Herrmann, S.X. Li, Potentiometric Sensor for Real-Time Monitoring of Multivalent Ion Concentrations in Molten Salt, Idaho Natl. Lab., 2010, pp. 1–10. INL/CON-10-17752.
[11] H. Lambert, Study of a Double Bubbler for Material Balance in Liquids, Idaho Natl. Lab., 2013, pp. 1–85. INL/EXT-13-29609.
[12] A.N. Williams, G.G. Galbreth, J. Sanders, Accurate determination of density, surface tension, and vessel depth using a triple bubbler system, J. Ind. Eng. Chem. 63 (2018) 149–156.
[13] M.M. Tylka, J.L. Willit, J. Prakash, M.A. Williamson, Method development for quantitative analysis of actinides in molten salts, J. Electrochem. Soc. 162 (9) (2015) H625–H633.
[14] S.R. Pouri, M. Manic, S. Phongikaroon, An interactive reverse-engineering cyclic voltammetry for uranium electrochemical studies in LiCl-KCl eutectic salt, Nucl. Technol. 197 (3) (2017) 308–319.
[15] H. Andrews, S. Phongikaroon, Electrochemical and laser-induced breakdown spectroscopy signal fusion for detection of UCl_3-$GdCl_3$-$MgCl_2$ in LiCl-KCl molten salt, Nucl. Technol. (2020) 1–10.
[16] A. Williams, S. Phongikaroon, Laser-Induced breakdown spectroscopy (LIBS) measurement of uranium in molten salt, Appl. Spectrosc. 72 (7) (2018) 1029–1039.
[17] A. Williams, B. Keith, S. Phongikaroon, Measurement of cerium and gadolinium in solid lithium chloride–potassium chloride salt using laser-induced breakdown spectroscopy (LIBS), Appl. Spectrosc. 71 (10) (2017) 2302–2312.
[18] Ammon N. Williams, Supathorn Phongikaroon, Laser-induced breakdown spectroscopy (LIBS) in a novel molten salt aerosol system, Appl. Spectrosc. 71 (4) (2017) 744–749.
[19] P.L. Lafreniere, D.S. Rappleye, R.O. Hoover, M.F. Simpson, E.D. Blandford, Demonstration of signature-based safeguards for pyroprocessing as applied to electrorefining and the ingot casting process, Nucl. Technol. 189 (2) (2015) 173–185.
[20] C.L. Murphy, Report on Concepts & Approaches for SSBD for eCHEM, Los Alamos Natl. Lab., 2016, pp. 1–13. LA-UR-16-27463.
[21] D. Rappleye, S.M. Jeong, M.F. Simpson, Application of multivariate analysis techniques to safeguards of the electrochemical treatment of used nuclear fuel, Ann. Nucl. Energy 77 (2015) 265–272.
[22] D. Rappleye, M.F. Simpson, R. Cumberland, D. McNelis, M.S. Yim, Simulated real-time process monitoring of a molten salt electrorefiner, Nucl. Eng. Des. 273 (2014) 75–84.
[23] A. Shannon, M.F. Simpson, Simulated response to process abnormalities during spent nuclear fuel electrorefining, Ann. Nucl. Energy 110 (2017) 1002–1009.
[24] R.M. Cumberland, M.S. Yim, Development of a 1D transient electrorefiner model for pyroprocess simulation, Ann. Nucl. Energy 71 (2014) 52–59.
[25] Y. Sakamura, T. Murakami, K. Tada, S. Kitawaki, Electrowinning of U-Pu onto inert solid cathode in LiCl-KCl eutectic melts containing UCl_3 and $PuCl_3$, J. Nucl. Mater. 502 (2018) 270–275.
[26] Y.E. Jung, M.S. Yim, Experimental studies of lanthanides electro-codeposition in molten salt to evaluate a 1-D electrorefining computer model, J. Electrochem. Soc. 167 (2020), 142501.
[27] J.A. Howell, H.O. Menlove, C. Rodriguez, D. Beddingfield, A. Vasil, J.E. Brown, C. Baumgart, Video Time Radiation Analysis Program (VTRAP)-Requirements and Preliminary Design Document, Los Alamos Natl. Lab., 1994, pp. 1–14. NIS-7/94-995.
[28] N. Shoman, B.B. Cipiti, Unsupervised Machine Learning for Nuclear Safeguards, Sandia Natl. Lab., 2018, pp. 1–10. SAND2018-5996C.
[29] B.B. Cipiti, F.A. Durán, B. Key, Y. Liu, I. Lozano, R. Ward, Modeling and Design of Integrated Safeguards and Security for an Electrochemical Reprocessing Facility, Sandia Natl. Lab., 2012, pp. 1–49. SAND2012-9303.
[30] S.R. Pouri, M. Manic, S. Phongikaroon, A novel framework for intelligent signal detection via artificial neural networks for cyclic voltammetry in pyroprocessing technology, Ann. Nucl. Energy 111 (2018) 242–254.
[31] R.O. Hoover, D.S. Yoon, S. Phongikaroon, Effects of temperature, concentration, and uranium chloride mixture on zirconium electrochemical studies in LiCl-KCl eutectic salt, J. Nucl. Mater. 476 (2016) 179–187.
[32] ASTM, Standard Test Method for Coulometric Reduction of Surface Films on Metallic Test Samples, American Society for Testing and Materials, West Consohocken, PA, 2013.
[33] A.J. Bard, L.R. Faulkner, Electrochemical Methods: Fundamentals and Applications, second ed., John Wiley & Sons, Inc., New York, 2001.
[34] E. Soria, J. Martin, R. Magdalena, M. Martinez, A. Serrano, Handbook of Research on Machine Learning Applications, Chapter L. Torrey and J. Shavlik, Transfer Learning, IGI Global, 2009.
[35] Y. Shibuta, Y.S. Unoura, T. Sato, H. Shibata, M. Kurata, T. Suzuki, A phase-field simulation of uranium dendrite growth on the cathode in the electrorefining process, J. Nucl. Mater. 414 (2) (2011) 114–119.